Theory of electron transport through single molecules of polyaniline

2007 J. Phys.: Condens. Matter 19 215204

(http://iopscience.iop.org/0953-8984/19/21/215204)

IOP PUBLISHING JOURNAL OF PHYSICS: CONDENSED MATTER

J. Phys.: Condens. Matter **19** (2007) 215204 (16pp) doi:10.1088/0953-8984/19/21/215204

Theory of electron transport through single molecules of polyaniline

Myeong H Lee[1], Gil Speyer[2] and Otto F Sankey[1]

[1] Department of Physics, Arizona State University, Tempe, AZ 85287-1504, USA
[2] Fulton High Performance Computing Center, Arizona State University, Tempe, AZ 85287-1504, USA

Received 28 November 2006, in final form 11 January 2007
Published 1 May 2007
Online at stacks.iop.org/JPhysCM/19/215204

Abstract

We present theoretical results for the electron transport properties of the organic molecule polyaniline, especially leucoemeraldine (LEB), the fully reduced form. The electron tunnelling characteristics of these chain-like molecules are described by their complex band-structure. We explore how the bandgap and tunnelling decay parameter β depend on the oxidation state of the molecule and on the torsion angle between rings. It is found that the metal Fermi level lies near the HOMO for gold contacts with a single leucoemeraldine molecule, which results in non-linear I–V characteristics. The conductance of a hepta-aniline (LEB) oligomer is obtained from a first-principles I–V curve and compared with the recent experimental results. We examine the effect of stretching of the molecule on its conductance to explain the discrepancy between the theoretical simulations and single-molecule conductance measurement experiment.

1. Introduction

Polyaniline refers to a family of polymers where nitrogen is a link between two carbon 6-rings. The result is to produce long polymer chains of variable length. Their unusual electronic properties and variety of form is a consequence of nitrogen's variable bonding arrangement. Acid/base interactions change the bonding of the linking N; it can be in either its reduced state containing the amine form (C–HN–C entities) or in the oxidized state containing the imine form (C–N=C entities). The three main laboratory forms are shown in figure 1. Leucoemeraldine base (LEB) is fully reduced, containing only the C–NH–C amine (figure 1(a)). Here the carbon 6-rings are phenyl rings with resonantly bonded carbon as in benzene. The half-oxidized form is the emeraldine base (EB), where half the nitrogen is oxidized in the imine form with nitrogen–carbon double bonds (figure 1(b)). The carbon 6-rings also change character and one-quarter of them become quinoids containing carbon double bonds. The fully oxidized form is pernigraniline base (PNB), containing all imine nitrogen, and the carbon 6-rings are one-half phenyl and one-half quinoid rings (figure 1(c)).

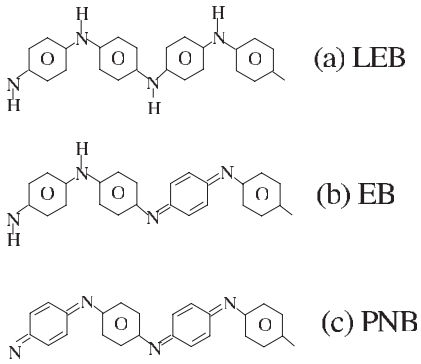

Figure 1. Schematic diagram of polyaniline: (a) leucoemeraldine base (fully reduced form), (b) emeraldine base (half-oxidized form) and (c) pernigraniline base (fully oxidized form).

Polyaniline has been widely studied for its property as a bulk conducting polymer. The importance of polyaniline as a conducting polymer results from the insulator–metal transition (conductivity increase up to 10 S cm^{-1}) brought about by electrochemical oxidation of leucoemeraldine base or acidic treatment of emeraldine base [1–5], which is presumably because of the unfilled band caused by the removal of an electron producing an open shell system. Polyaniline has also attracted interest for its technical applications such as battery devices and films [6, 7]. Much is known about the electrical conductivity of bulk materials, but the conductivity of single-molecular species has only recently been probed [8, 9]. There have been various theoretical approaches to determine the electronic and structural properties of polyaniline such as extended Hückel theory (EHT) [10], the valence effective Hamiltonian (VEH) technique [11–15], *ab initio* calculations based on density functional theory (DFT) [16–19], or Car–Parrinello molecular dynamics [20, 21]. In addition, there has been research to explain the effect of protonation [22–24] and the conduction mechanism [25–28] of polyaniline.

Leucoemeraldine base (LEB), containing only phenyl rings connected by an amine nitrogen, is known to be an insulator with a bandgap of ∼3.6 eV [29, 30]. There has been much research concerning its electronic band-structure [11, 16, 20, 31, 32], and the chain-length dependence [14] of its electronic and optical properties. Additionally, the torsion angle dependence of its electronic properties [12, 33] has been studied.

In this paper we investigate the electron transport properties of LEB based on first-principles calculations of ballistic electron transport through single molecules. An understanding of the electron transport properties of the neutral fully reduced form of polyaniline provides a useful foundation for understanding transport through this wide class of technologically important molecules.

A brief outline of the paper follows. In section 2 we describe the theoretical techniques used to investigate the electronic states of polyaniline. Electron transport through single molecules with a 'wide' HOMO–LUMO gap like LEB is usually via a tunnelling mechanism. The tunnelling current becomes exponentially small for long molecules ($e^{-\beta x}$), and the single most important quantity that characterizes the tunnelling is the exponential decay parameter β. In section 3 the complex band-structure technique is used to determine β for all energies in the HOMO–LUMO gap. Additionally, we investigate how the bandgap and decay parameter β vary with the torsion angle. The current observed for a single molecule in contact with metal leads will depend on where the Fermi level of the metal lines up with the HOMO–

LUMO levels of the molecule. In section 4 we determine the Fermi level alignment between HOMO and LUMO levels by constructing interfacial contacts of a model metal/molecule/metal system. Sections 3 and 4 give us the two most important parameters for electron transport—the alignment of the Fermi level, and the decay parameter β. From just these two pieces of information we are able to make a rough estimate for the conductance of the hepta-aniline oligomer. This is done in section 5. In section 6 we perform a proper calculation of the I–V curve of the hepta-aniline oligomer using density functional theory (DFT) Green's function scattering methods. First-principles calculations have shown good agreement with the single-molecule conductance measurement experiments for many molecules [34–37]. Our calculation on the conductance of hepta-aniline oligomer is compared with our simple estimate and with the result of a single-molecule conductance measurement experiment [9]. In section 7 we investigate stretching of the molecule which may occur during the conductance measurement. We compute the I–V curve for the stretched molecule and compare the conductance with the experimentally measured value. Also the decay parameter at the Fermi level is determined to obtain a rough estimate for the conductance of the stretched molecule. Finally, in section 8 we summarize our results.

2. Theoretical methods

We begin with a description of the theoretical methods used. We sequentially describe (i) the electronic structure methods used, (ii) the complex band-structure method to determine the tunnelling states, and (iii) the calculation of an I–V curve using a Green's function approach.

The primary electronic structure method used is Fireballs-2000 [38], which uses local-orbital density functional theory and pseudopotentials. All the calculations were performed using a minimal basis set (s for H, sp^3 for C and N). We compare our results with other computational methods for complex band-structure (PWSCF) [39] and Fermi level alignment (VASP)[3], both being DFT plane-wave pseudopotential methods.

We next describe the calculation of the complex band-structure. The complex band-structure gives deep insights concerning the intrinsic conduction properties of a periodic molecule, such as polyaniline. For an infinitely long periodic system, only real Bloch k vectors are allowed, and the resulting $E(k)$ relation produces the conventional band-structure. The reason that only real k vectors are allowed is because at large distances the wavefunction blows up: if not in the positive x-direction then in the negative x-direction. Such states are not normalizable, and thus not allowed. It is important to realize, however, that states with imaginary k vector satisfy the Schrödinger equation—we infrequently use them because of the boundary condition (at $\pm\infty$). The situation is quite different for molecules with finite length. Bloch states with imaginary k vectors are the evanescent states that describe tunnelling of the electron through the molecule. They are the same solutions of the periodic molecule that always existed but now become physically relevant due to changing of the boundary conditions.

The tunnelling probability of the electrons starting in one metal contact with an energy within the molecule's bandgap is proportional to $e^{-\beta L}$, where β is defined as $2 \times \mathrm{Im}[k]$ and L is the length of the molecule. The factor of 2 is just from squaring the wavefunction to produce a probability. Thus we have effectively solved the tunnelling problem if we find the imaginary k vectors. To do this, we extend our periodic molecule to have an infinite length, for which finite segments are the molecules of our interest. Then the electronic energy eigenstates are taken to have the Bloch form, $\psi(x) = e^{ikx}u(x)$, where $u(x)$ has the periodicity of the system.

[3] The Vienna *Ab Initio* Simulation Program (VASP) was developed at the Institut für Theoretiche Physik of the Technische Universität Wien: [40].

We rewrite the Schrödinger equation as an eigenvalue equation for λ, where $\lambda = e^{i(k_0+i\beta/2)a}$ and a is the lattice constant. We consider the energy as an input and obtain the eigenvalues λ to yield the given energy [41]. Details can be found in [41–43].

The complex band-structure is for an infinite periodic system. Polyaniline consists of a sequence of repeating units. We let B denote a benzene ring and Q a quinoid ring. Schematically the periodicity of LEB is indicated as $\cdots$–(N–B–N–B)–(N–B–N–B)–$\cdots$, where the repeat unit is N–B–N–B–. The zigzag nature of the chain requires a pair of benzene ring/nitrogen units (see figure 1(a)). Similarly, EB (figure 1(b)) is $\cdots$–(N–B–N–B–N=Q=N–B)–$\cdots$ and PNB is $\cdots$–(N=Q=N–B)–(N=Q=N–B)–$\cdots$ (figure 1(c)). Therefore, figure 1 shows two unit cells for LEB and PNB, and one unit cell for EB.

Finally, we describe the calculation of an I–V curve of a single molecule attached to a pair of metal electrodes. The metal contacts that we use are a pair of (111) gold slabs. The coupling matrix elements that connect the metal to the molecule are obtained from a supercell calculation with six atomic layers of gold. Our method is a Green's function based method of the transition probabilities from one metal contact to the other, and reduces to Landauer theory [44], where the conductance is considered as a quantum mechanical transmission of electrons through a barrier. The current is determined by summing all the contributions from the occupied scattering states of both electrodes under bias [34, 45–49]. The supercell system is periodic both along the molecular axis and in perpendicular directions. Bloch's theorem is used to obtain the necessary Hamiltonian and overlap matrix elements. The gold slabs with finite thickness are transformed into semi-infinite bulk electrodes by use of the block recursion method [34, 50]. We calculate interactions between orbitals such as molecule–molecule and molecule–electrodes interactions self-consistently at zero voltage.

3. Complex band-structure

The complex band-structure determines the exponential decay of the tunnelling current through a molecule as a function of energy [41, 51]. The decay parameter $\beta(E)$ is defined as $2 \times \mathrm{Im}[k]$ of the Bloch k vector, and the tunnelling probability is $|\psi|^2 \approx e^{-\beta L}$, where L is the length of the molecule. The energy E to be used for small bias is the Fermi energy E_F of the metal, which aligns itself in the HOMO–LUMO gap of the molecule (see section 4). Knowledge of the decay parameter can also be used to produce a rough estimate of the conductance of the molecule.

All the bond lengths and bond angles of LEB (figure 1(a)) were optimized using quantum chemistry Hartree–Fock[4] with the 6-31+G(d, p) basis at the restricted Hartree–Fock (RHF) level. The optimized structure shows that all the nitrogen atoms lie in the same plane. All the *para*-carbon atoms connected to nitrogen and hydrogen atoms linked to the nitrogen are coplanar with the nitrogen atoms. (The *para*-carbon atom in the phenyl ring is the carbon atom linked to the nitrogen atom and *ortho*-carbon atoms are positioned between *para*-carbon atoms within the phenyl ring.) Also, all the carbon atoms on a phenyl ring reside on a plane, but not the same plane as the N-atoms. The two phenyl rings B_1 and B_2 of the unit cell (N–B_1–N–B_2)– are twisted about nitrogen and in opposite directions from each other with a torsion angle of 29°. The torsion angle is defined as an angle between the phenyl ring and the plane of the nitrogen atoms. The rotation of the phenyl rings in opposite directions is produced by repulsive steric interactions occurring between hydrogen atoms on adjacent phenyl rings. The torsion angle that we obtained is close to that found by others [12, 14].

[4] The General Atomic and Molecular Electronic Structure System (GAMESS) is an *ab initio* quantum chemistry package. The version of GAMESS that we used is described in [52].

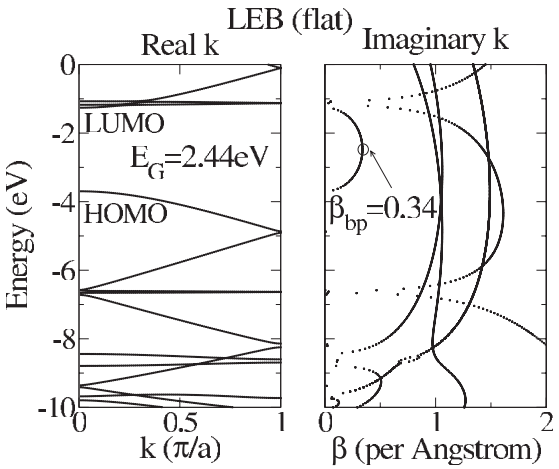

Figure 2. Complex band-structure of flat leucoemeraldine base (LEB); the left figure shows a conventional band-structure with real k, and in the right region β ($2 \times \mathrm{Im}[k]$ of Bloch k vector) versus energy is plotted. The tunnelling current decreases as $|\psi|^2 \approx \mathrm{e}^{-\beta L}$, where L is the length of the molecule. The semi-elliptical curve in the bandgap region gives the most penetrating states, and β_{bp} is defined as a peak point of this curve.

We examined the complex band-structure of LEB for both a flat structure (all the atoms in the same plane) as well as for the optimized structure (two phenyl rings twisted against each other by 29°). In π-bonded organics, the frontier orbitals are often dominated by π bonding and we wanted to compare the ideal system where all π orbitals are in the same plane to the real system where they are not in the same plane.

Figures 2 and 3 show the complex band-structure of LEB for flat and twisted structures. LEB flat and twisted structures have similar bandgaps E_{g} between the HOMO and LUMO of 2.44 and 2.66 eV, respectively at $k = 0$. This is lower than the experimentally measured value (∼3.6 eV) [29, 30], which is not unexpected in DFT calculations. The eigenvector of the LUMO band shows that the dominant orbitals are the *ortho*-carbon atom π orbitals and there is little contribution from *para*-carbon atom orbitals and nitrogen π orbitals. This prevents π interaction between the unit cells and results in flatness of the band. The HOMO band is mostly dominated by nitrogen atom π orbitals. These features are in agreement with other theoretical studies [13].

The effect of torsion of the phenyl ring on the bandgap seems not to be a large effect (∼9%). There has been research about the effect of torsion angle on the bandgap [12]. Brédas *et al* increased the torsion angle of the two adjacent phenyl rings ($T = |\theta_1| + |\theta_2|$) from 60° to 90° without any torsion angle dimerization ($|\theta_1| = |\theta_2|$), and the bandgap increased from 3.77 to 4.20 eV (∼11% change). Our results show that the bandgap increases from 2.65 eV ($T = 60°$) to 2.93 eV ($T = 90°$) (∼11% change) (figure 4). They also varied the torsion angle of two adjacent phenyl rings (θ_1, θ_2) differently while keeping $|\theta_1| + |\theta_2|$ the same. They found that the bandgap of LEB changes by less than 10% by the torsion angle dimerization ($\Delta\theta$).

Comparing the imaginary k vectors of figure 2 (flat) and figure 3 (twisted) shows a surprisingly large difference. These figures show many imaginary k vectors; we need to focus only on the important parts. First, the important energy region is between the HOMO and the LUMO. Second, within this energy region there are many imaginary k vectors. What is of interest is the imaginary k vector of the smallest magnitude. This band produces the highest probability of tunnelling. The smallest β values branch is a 'semi-elliptical' curve

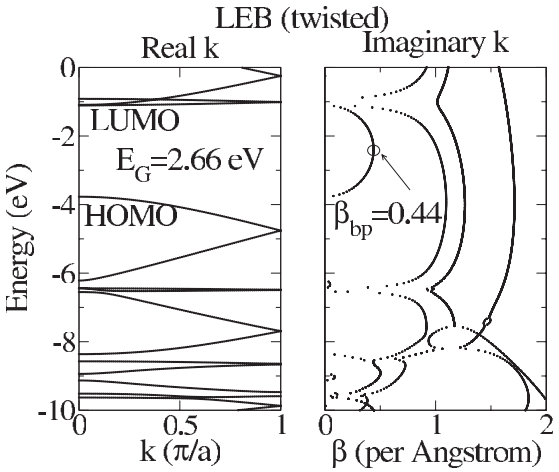

Figure 3. Complex band-structure of twisted leucoemeraldine base (LEB); the bandgap is similar to that of the flat LEB, but the decay parameter β is much larger in the twisted LEB.

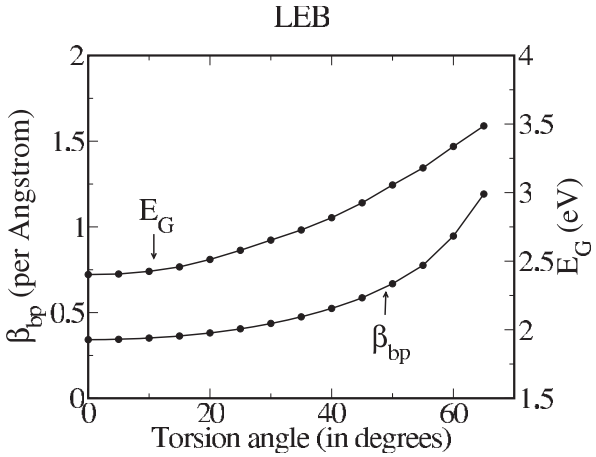

Figure 4. The decay parameter at branch point (β_{bp}) and the bandgap (E_{G}) of leucoemeraldine with increasing torsion angle.

connecting the HOMO to a (near) LUMO band. The 'branch point' is the energy at which β is maximum; electrons at this energy (from the metal) produce the least penetrating tunnelling through the molecule. There are other semi-elliptical curves connecting distant bands, but these are tunnelling through very tall 'barriers' and produce a rapid tunnelling decay.

We find that the maximum β is 0.34 $\mathrm{\AA}^{-1}$ for the flat structure versus 0.44 $\mathrm{\AA}^{-1}$ for the twisted structure. This is a $\sim$29% change; however, this is in the exponent, which means a hypothetical flat structure is far more conductive than the true twisted structure. From a 'barrier' point of view, the bandgap has only changed by about 10%, and a 30% change of β is surprising. This is especially true in simple models where we view β as scaling as the $\sqrt{E}$; the $\sqrt{E}$ behaviour should produce a dull effect. However, from a chemical point of view, one would argue that the π-orbital alignment of the flat structure should greatly enhance conduction; this qualitative view agrees with our finding. One unit cell of the molecule is

10.65 Å long (flat) and 10.23 Å (twisted), so a β of 0.34 $Å^{-1}$ for the flat structure gives a decay of $e^{-0.34\ Å^{-1}\times 10.65\ Å} = 0.027$, while for the twisted structure $\beta_{bp} = 0.44\ Å^{-1}$ gives a decay of 0.011.

Higher β_{bp} of the twisted structure compared with the flat structure shows that torsions of the phenyl rings are important in determining the electron transport properties of polyaniline. To see how the torsion angle affects the bandgap E_g and decay parameter at the branch point β_{bp}, we compute the complex band-structure with varying torsion angles. Figure 4 shows that both E_g and β_{bp} increase as the torsion angle increases. The effect becomes more pronounced at large torsion angles. The torsion angle for the optimized structure is 29°.

The complex band-structures just described used local orbitals and should accurately describe 'through bond' tunnelling. However, it may not include 'through space' tunnelling (i.e. vacuum tunnelling). As a check, we computed the complex band-structure using a plane-wave basis method (PWSCF) [39], which treats both forms of tunnelling on an equal footing. Using plane-wave LDA-DFT pseudopotentials we obtain $E_G = 2.3$ eV, $\beta_{bp} = 0.33\ Å^{-1}$ for the flat structure and $E_G = 2.5$ eV, $\beta_{bp} = 0.43\ Å^{-1}$ for the twisted structure. No additional vacuum tunnelling states are seen in the bandgap region. Overall, the results are quite similar to the local orbital Fireball calculations.

To investigate how the oxidation state of polyaniline affects the bandgap and decay parameter, we compute the complex band-structure of EB (half-oxidized form) and PNB (fully oxidized form). The optimized structure of EB and PNB was obtained using Hartree–Fock [52] with the STO-3G basis at RHF level. The relaxed structure of EB, composed of three benzene rings and one quinoid ring (–N–B–N–B–N=Q=N–B–), shows that the torsion angle of the quinoid ring is small (∼2°) while the two benzene rings adjacent to the quinoid ring leave the plane defined by the nitrogen atoms by a large torsion angle (∼63°) to reduce the steric hindrance. Another benzene ring (the leftmost phenyl ring in figure 1(b)) has relatively small torsion angle (∼8°) compared to the two other phenyl rings adjacent to the quinoid ring. The relaxed PNB (–N=Q=N–B–) shows that the quinoid ring almost stays in the plane (∼3°) while the benzene ring comes out of the plane by ∼64° torsion angle. Overall results for torsion of the rings are in agreement with the calculation by others [12, 14].

The unit cell of EB has size twice as large as that of LEB (half-size in k-space) and has two electrons taken off. As a result, the real band-structure of EB becomes flatter (the top valence band of LEB is folded back and split into HOMO and LUMO bands in EB) and shows a smaller bandgap, $E_G = 1.13$ eV, at $k = \pi/a$ (figure 5). The wavefunction of the HOMO is localized mostly at the amine nitrogen atoms (and a small contribution from carbon atoms in the benzene rings), and the wavefunction of the LUMO is localized at the imine nitrogen atoms (and a small contribution from carbon atoms in the quinoid ring).

Since the PNB is short of two electrons per unit cell compared to LEB, the top valence band of LEB becomes unoccupied and the second highest valence band becomes the HOMO band in PNB. Also, the alternation of the bond length between carbon and nitrogen atoms due to double and single bonds and the torsion angle dimerization by 3° and 64° (for the quinoid and benzene rings, respectively) leads to the opening of the gap at the band edge ($k = \pi/a$) as explained by Brédas *et al* [12]. It results in a bandgap of $E_G = 1.83$ eV (figure 6). The bandgap that we obtained is lower than the experimental value for both EB and PNB; $E_G = \sim 2$ eV for EB and ∼2.3 eV for PNB [30, 53].

The band-structure for imaginary k vectors shows that the decay parameter at the branch point β_{bp} is 0.44 and 0.55 $Å^{-1}$ for EB and PNB, respectively (figures 5 and 6). The decay parameter β_{bp} of EB is similar to that of LEB ($\beta_{bp}^{LEB} = 0.44\ Å^{-1}$) and β_{bp} of PNB is greater than that of LEB. Note that the bandgap (energy barrier) is greatest in LEB.

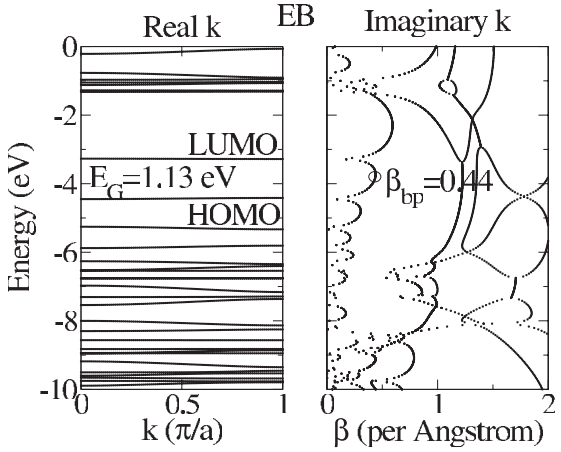

Figure 5. Complex band-structure of emeraldine base (EB); the real band-structure shows flattened bands and the bandgap decreases. The decay parameter at branch point β_{bp} is similar to that of the twisted LEB.

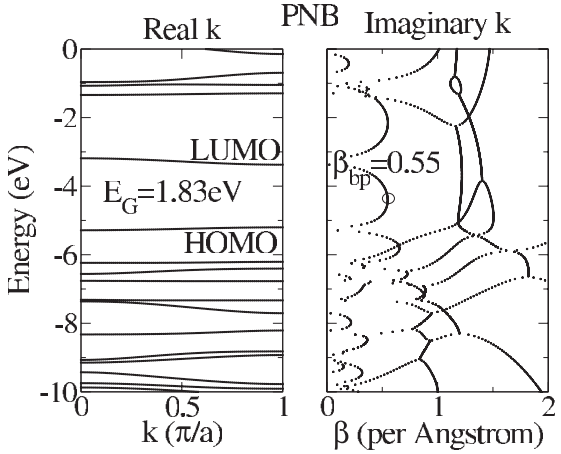

Figure 6. Complex band-structure of pernigraniline base (PNB); both the bandgap and decay parameter increase compared to EB.

These results show clearly that the bandgap alone is not the controlling factor in determining the tunnelling decay parameter.

4. Fermi level alignment

In the previous section we obtained the exponential decay parameter β for energies in the HOMO–LUMO gap of LEB (and PNB and EB). To know what value to use for a specific metallic contact we must know how the Fermi level of the metal is aligned with the molecular energy levels. Only electrons near the Fermi level contribute to molecular tunnelling when the molecule is sandwiched between metal electrodes. When the Fermi level is located near the branch point (near the middle of the HOMO–LUMO gap) the decay parameter $\beta(E_F)$ will be largest, yielding a low conductance or high resistance. Of course, as the Fermi level nears the HOMO or LUMO, β decreases and the conductance increases dramatically.

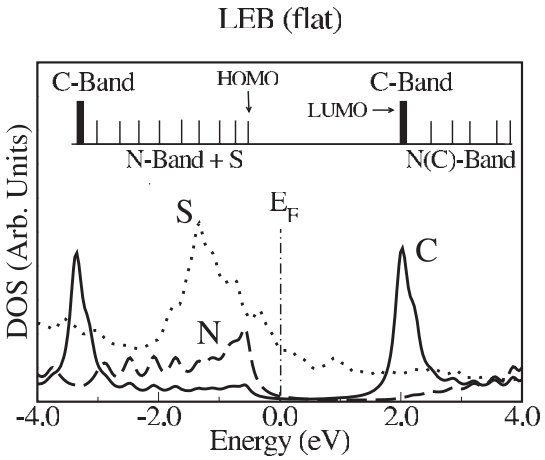

Figure 7. Projected densities of states per atom onto carbon, nitrogen, and sulfur atoms for flat leucoemeraldine base (LEB); the Fermi level is adjusted to zero. The upper part shows the energy bands of the isolated molecule.

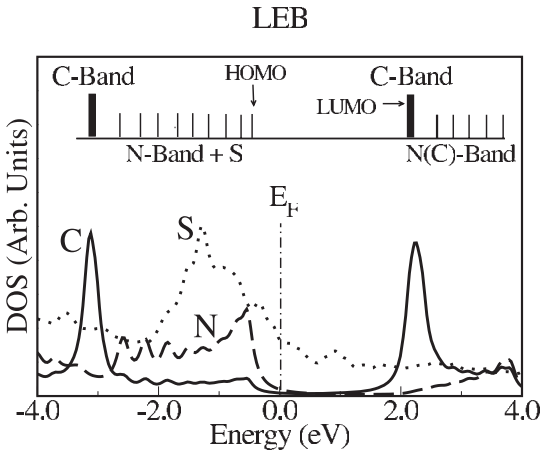

Figure 8. Projected densities of states per atom onto carbon, nitrogen, and sulfur atoms for twisted leucoemeraldine base (LEB); the HOMO is dominated by nitrogen orbitals, and the LUMO is dominated by carbon orbitals.

We determine the Fermi level alignment for the LEB/gold system. This is accomplished by computing the electronic states of a supercell containing a gold/molecule junction. The molecule is composed of eight phenyl rings interconnected by nitrogen atoms (a hepta-aniline oligomer). The terminal –NH groups on both ends of the molecule are removed and sulfur is attached. The sulfur attached to the molecule is positioned on the hollow site of the (111) gold slabs, which laterally form a supercell of 3×3 and are six Au layers deep. The hollow site is equidistant from three Au atoms on a Au surface. The distance between the sulfur and the hollow site was 1.9 Å, and the (Au-hollow-site, S, C) bond angle was 110° [36].

The Fermi level line-up is obtained from the electronic projected densities of states. Both plane-wave methods (VASP (see footnote 3)) and local orbital methods (Fireballs [38]) were used. The final Fermi level line-ups that are found are almost identical in the two methods, even though the computational methodologies were quite different. Figures 7 and 8 show the

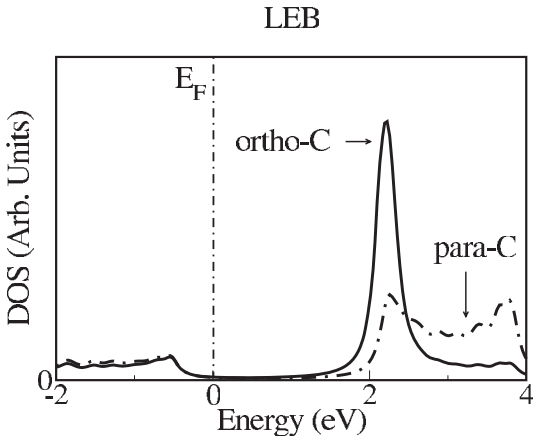

Figure 9. Projected densities of states per atom onto *ortho*-carbon atoms and *para*-carbon atoms for LEB twisted structure (LEB flat structure shows a similar tendency); *ortho*-carbon atom orbitals give the most contribution to the LUMO.

projected densities of states per atom onto the orbitals of nitrogen, carbon, and sulfur atoms. The flat and optimized (twisted) LEB structures are considered. The energies shown in the figures are all relative to the self-consistently determined Fermi level, which is adjusted to zero in both cases. The Fermi level E_F is not aligned near mid-gap but is aligned much closer to the HOMO in both cases. The HOMO is dominated by nitrogen atom orbitals while carbon atom orbitals dominate the LUMO. In the upper region of the figures the energy levels of the isolated molecule are shown. Comparing these with the atom-projected DOS of the metal/molecule/metal system, it is seen that the energy levels of the molecule persist (but broaden) after the molecule is attached to the metal.

We compared the projected densities of states onto *ortho*-carbon atoms and *para*-carbon atoms (figure 9). The result is that *ortho*-carbon atom orbitals give a much larger contribution to the LUMO than do the *para*-carbon orbitals. This is consistent with the result of eigenvector analysis explained in the previous section.

We also calculated the Fermi level alignment for EB and PNB (figures 10, 11). The projected densities of states show that the Fermi level lies near mid-gap for EB and slightly above mid-gap closer to the LUMO for PNB.

5. Simple estimate of conductivity

A simple estimate of the conductivity of LEB can be made once we know $\beta(E)$ from the complex band-structure and the energy E at which the E_F of the metal resides. We approximate the conductance (G) for the molecule of length L by

$$G \approx G_0 e^{-\beta(E_F)L}, \tag{1}$$

where G_0 is the quantum of conductance ($G_0 = 77\ \mu$S). This is clearly a crude estimate and can be no better than an order of magnitude estimate. However, even sophisticated calculations are usually no better than an order of magnitude when compared to experiment; such simple estimates can be used to rationalize which organic molecules should be good or bad conductors, and how geometrical alterations can be expected to change their conductance properties.

The complex band-structure of LEB flat and twisted structure shows that the decay parameter at the Fermi level $\beta(E_F)$ is 0.28 Å^{-1} for flat and 0.34 Å^{-1} for twisted structure

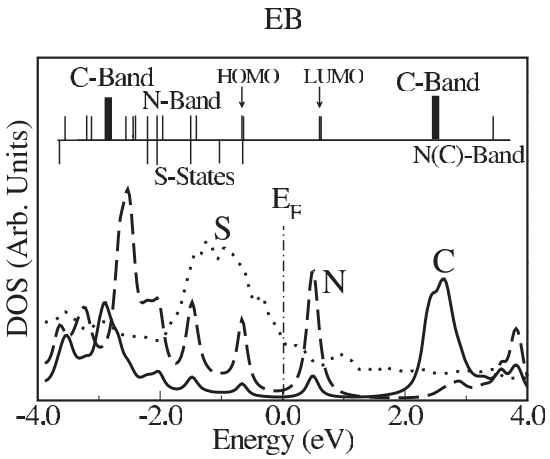

Figure 10. Projected densities of states per atom onto carbon, nitrogen, and sulfur atoms for emeraldine base (EB); the gold Fermi level is aligned near mid-HOMO–LUMO-gap.

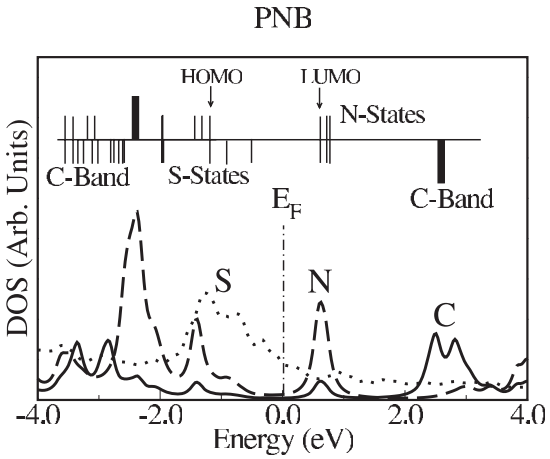

Figure 11. Projected densities of states per atom onto carbon, nitrogen, and sulfur atoms for pernigraniline base (PNB); the gold Fermi level is indicated.

(figures 2, 3). Thus our conductance estimates are $G = 0.51$ nS for the flat structure and $G = 0.073$ nS for the twisted structure for hepta-aniline. Notice that the optimized (twisted) structure is one-seventh as conductive as the flat structure.

The value of $\beta(E_F)$ is sensitively dependent on the Fermi level E_F for energies not near the branch point. To illustrate how important the Fermi-level alignment is, let us give a 'poorer' estimate and use a near mid-gap energy instead. This means we use β_{bp} of 0.34 $Å^{-1}$ (flat) and 0.44 $Å^{-1}$ (optimized) instead. The results for the conductance are $G = 0.039$ nS for flat structure and $G = 0.0012$ nS for twisted structure for the hepta-aniline. These are much smaller than 0.51 and 0.073 nS by a factor of ∼13 and ∼61 when using $\beta(E_F)$ for flat and twisted hepta-aniline. This shows that, no matter how sophisticated a calculation is, the final result is no better than its estimate of where the Fermi level is since the conductance is exponentially sensitive to β at this energy. We believe far too little attention has been paid to this point.

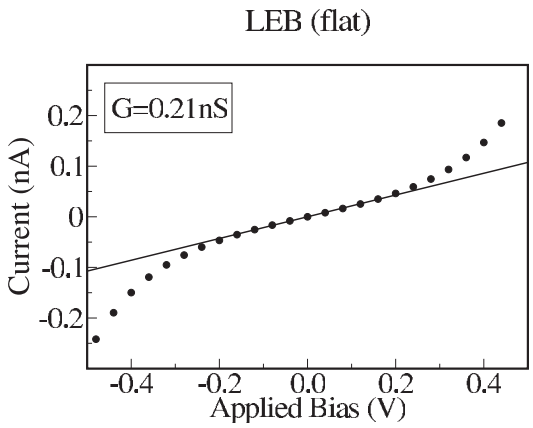

Figure 12. I–V curve for LEB flat structure; the conductance ($G = 0.21$ nS) was calculated for the linear region.

The values $G = 0.51$ nS for the flat structure and $G = 0.073$ nS for the twisted structure for the hepta-aniline are rough estimates for conductance of the molecule. These estimates did not require any 'special' solutions to transport equations, just a complex band-structure and a Fermi-level alignment calculation. In the next section, we will yield the conductance from a Green's function I–V method and compare it with the result from equation (1).

We also calculated the conductance for EB and PNB using the decay parameter at the Fermi level ($\beta(E_F) = 0.44$ Å^{-1} for EB and 0.50 Å^{-1} for PNB). The Fermi levels are shown in figures 10 and 11. The conductance estimates are $G = 1.7$ pS for EB and $G = 0.75$ pS for PNB of hepta-aniline. Thus EB and PNB are far less conductive ($\sim 10^{-2}$ less) than LEB.

6. I–V calculation

The current–voltage calculations for a hepta-leucoemeraldine oligomer are determined using DFT Green's function scattering methods [44]. The linear region near zero bias yields the conductance for the metal–molecule–metal system [34]. The calculation already has the Fermi-level alignment built in since it uses a coupled metal–molecule–metal system. Since the Fermi level does not lie in the middle of the bandgap, the I–V curve shows considerable nonlinearity (figures 12 and 13). The conductance in the linear region was 0.21 nS for the flat structure (figure 12) and 0.043 nS for the twisted structure (figure 13).

A single-molecule conductance measurement experiment was performed for the same molecule [9], and the measured conductance was 0.32 nS, which is higher than the theoretically predicted value. Considering that the molecule will be twisted by some amount of torsion angle, our estimation for conductance is off by a factor of 7.4 from the experimentally measured value. A factor of 7.4 (G_{Exp}/G_{Th}) that we have obtained for LEB is generally higher than the error obtained for other molecules: alkanes (0.47–0.78) [34, 35], carotenoid polyenes (0.31–0.36) [36], photochromic molecules (1.7–2.4) [37] except benzenedithiol (0.02) [34, 54]. However, there are many factors that affect the conductance calculation—the binding site of the molecule on the Au surface, the orientation of the molecule (bond angle of Au–S–C) on the Au surface, the distance between the sulfur atom and the Au surface, the contact geometry between the molecule and metal (planar contact or contact forming gold filament), etc. Considering all these factors and uncertainties, the discrepancy between the single-molecule conductance measurement and the first-principles calculation by an order of magnitude is not too surprising.

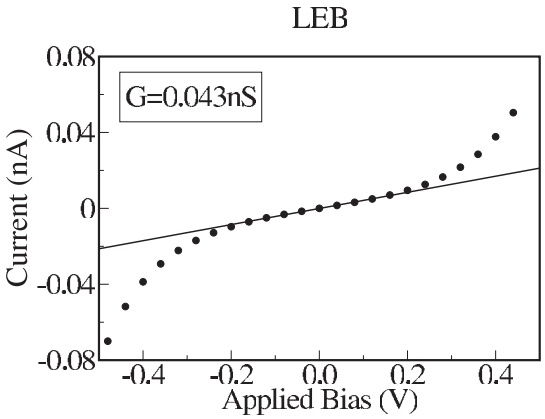

Figure 13. I–V curve for LEB twisted structure; the conductance ($G = 0.043$ nS) is decreased by a factor of five compared with flat structure.

The conductance from the I–V calculation was slightly larger than the simple estimates (equation (1)) for both flat and twisted structures; $G^{\mathrm{Est}}_{\beta(E_{\mathrm{F}})}/G_{IV} = 2.4$ and 1.7 for flat and twisted structures, respectively. Considering that the simple estimate of conductance using $\beta(E_{\mathrm{F}})$ was much higher than the conductance using β_{bp} by a factor of ∼13 and ∼61 for flat and optimized structures, it is consistent that the Fermi level of LEB is aligned near the band edge instead of near mid-gap. Both the I–V calculation and the simple estimate show that the flat structure is more conductive than the twisted structure ($G_{\mathrm{flat}}/G_{\mathrm{twisted}} = 4.9$ from the I–V calculation and 7.0 from the simple estimate).

7. Stretching

Previous experience shows that, when comparing experiment and theory, theory usually overestimates the conductance. Theoretical simulations make 'ideal' contacts, while in experiment they may be less than ideal. Also, other transport inhibitors may play a role in the experiment (i.e. inelastic scattering), but there are no inhibitors in the theory. Yet our Green's function simulation of the conductance underestimates the experimental value. Perhaps there is something more at work here.

The experimental conductance measurement of Chen *et al* [9] uses an STM break-junction method [35] to pull the molecule. As a result, the molecule may be distorted by the applied force. Usually this may produce small or modest effects, but the torsional twisting of polyaniline may be sensitive to stretching forces. Here we explore a planarization of the molecule caused by stretching the molecule. We find that it may explain why the experimentally measured conductance is greater than the theoretical value.

To see how stretching of the molecule changes its conductance, we stretched the molecule by fixing the end atoms using Hartree–Fock [52] with a 6-31G basis. Each of these stretched molecules is then successively placed between gold metal slabs and the conductance of the molecule is computed (figure 14). The force of stretching was calculated ($|F| = \mathrm{d}E/\mathrm{d}x$ where E is the total energy and $\mathrm{d}x$ is the stretched length for each step (0.2 Å)), and is of the order of nanonewtons in magnitude.

As the molecule is stretched, the most significant distortion is that two phenyl rings connected by a single nitrogen move further apart; this only requires a bond-bending of the C–N–C angle. As the two phenyl rings move apart, the steric interaction between hydrogen

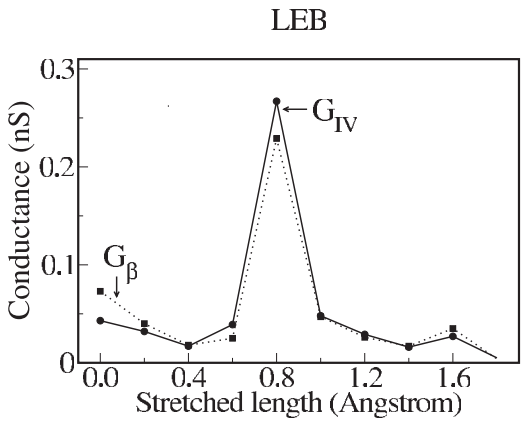

Figure 14. The conductance of LEB twisted structure with the stretched length; G_{IV} is obtained by I–V calculation, and $G_{\beta} \approx G_0 e^{-\beta(E_F)L}$. Both of them reach the maximum conductance at the stretching of 0.8 Å.

atoms on the phenyl rings decreases significantly, reducing the torque producing the torsion of the two rings. The torsion angle (angle between the phenyl ring and the plane defined by nitrogen atoms) decreases, reaches a minimum when stretched by 0.8 Å, and increases again. Of course, at some critical force the molecule will snap off the AFM tip and the current will drop to zero (or background).

The conductance computed during stretching of the molecule is shown in figure 14. The stretching is given as an overall stretch of the molecule (of unstretched length 10.23 Å). Of course, stretching order 1 Å does not mean that bond lengths stretch by this much; most of the stretch is in bond angles, specifically the C–N–C angle, and the length increase is obtained by flattening the molecule from its twisted configuration. The conductance shown in figure 14 has a complex behaviour that is difficult to understand in detail. But the clear peak near 0.8 Å is unmistakable. The maximum conductance (0.27 nS) was obtained for the stretched molecule by 0.8 Å, where the torsion angle becomes small enough to produce the increase in the length of the molecule. This value is much closer to the experimentally measured value 0.32 nS ($G_{\mathrm{Exp}}/G_{\mathrm{Th}} = 1.2$). Although this does not prove that the experimental measurement is that of a flat structure produced by stretching the molecule, it does offer a simple explanation for why the experimental value is so large compared to theory.

We also calculated the decay parameter of the molecule at the Fermi level and conductance (G_{β} using equation (1)) as it is stretched (figure 14). The complex band-structure needs as input only the structure of the molecule which is obtained from the Hartree–Fock quantum chemistry results. The Fermi level alignment was obtained by computing the projected density of states for each stretched molecule. The Fermi level was aligned near the HOMO in all cases. It is remarkable that a simple estimate calculation of the conductance tracks very well the Green's function I–V calculation (G_{IV}).

8. Conclusion

In this paper, we calculated the decay parameter and bandgap of leucoemeraldine by computing the complex band-structure. The geometry optimization shows that the molecule does not lie in the plane. Instead, two phenyl rings are twisted by about 29°, and the twist of the molecule makes the decay parameter at the branch point β_{bp} increase from 0.34 to 0.44 $\mathrm{Å}^{-1}$ while the

bandgap is mildly affected (2.44 versus 2.66 eV). The projected density of states shows that the Fermi level is aligned near the HOMO rather than being placed in the middle of the bandgap for both flat and twisted structures. The estimated conductance of hepta-aniline using the decay parameter at the Fermi energy ($\beta_{E_F} = 0.28$ and 0.34 $Å^{-1}$ for flat and twisted structure) was 0.51 and 0.073 nS, respectively.

We calculated the I–V curve of hepta-aniline using the DFT Green's function scattering method; the conductance from the I–V curve was 0.21 and 0.043 nS for flat and twisted structures. A single-molecule conductance measurement, however, shows that the conductance of hepta-aniline is higher than the theoretically predicted value ($G_{Exp} = 0.32$ nS) by a factor of 7.4. That the single-molecule conductance measurement experiment shows higher conductance could be explained by assuming that the molecule is stretched during the pulling process, which causes the molecule to twist with smaller torsion angle. As the stretching proceeds, the torsion angle of two phenyl rings decreases and the conductance of hepta-aniline reaches its maximum value, 0.27 nS. This is different from the experimental value by a factor of 1.2. This result shows that the stretching of the molecule during the pulling process can make a significant difference in conductance for a twisted molecule like leucoemeraldine.

References

[1] MacDiarmid A G, Chiang J C, Richter A F and Epstein A J 1987 *Synth. Met.* **18** 285
[2] Epstein A J, Ginder J M, Zuo F, Woo H-S, Tanner D B, Richter A F, Angelopoulos M, Huang W-S and MacDiarmid A G 1987 *Synth. Met.* **21** 63
[3] Epstein A J, Ginder J M, Zuo F, Bigelow R W, Woo H-S, Tanner D B, Richter A F, Huang W-S and MacDiarmid A G 1987 *Synth. Met.* **18** 303
[4] Ofer D, Crooks R M and Wrighton M S 1990 *J. Am. Chem. Soc.* **112** 7869
[5] Zuo F, Angelopoulos M, MacDiarmid A G and Epstein A J 1987 *Phys. Rev.* B **36** 3475
Zuo F, Angelopoulos M, MacDiarmid A G and Epstein A J 1989 *Phys. Rev.* B **39** 3570
[6] Kulkarni V G, Campbell J C and Mathew W R 1993 *Synth. Met.* **55–57** 3780
[7] Yang Y and Heeger A J 1994 *Appl. Phys. Lett.* **64** 1245
[8] He H, Zhu J, Tao N J, Nagahara L A, Amlani I and Tsui R 2001 *J. Am. Chem. Soc.* **123** 7730
[9] Chen F, He J, Nuckolls C, Roberts T, Klare J E and Lindsay S 2005 *Nano Lett.* **5** 503
[10] Euler W B 1986 *Solid State Commun.* **57** 857
[11] Boudreaux D S, Chance R R, Wolf J F and Shacklette L W 1986 *J. Chem. Phys.* **85** 4584
[12] Brédas J L, Quattrocchi C, Libert J, MacDiarmid A G, Ginder J M and Epstein A J 1991 *Phys. Rev.* B **44** 6002
[13] Libert J, Bredas J L and Epstein A J 1995 *Phys. Rev.* B **51** 5711
[14] Libert J, Cornil J, dos Santos D A and Brédas J L 1997 *Phys. Rev.* B **56** 8638
[15] Barta P, Kugler Th, Salaneck W R, Monkman A P, Libert J, Lazzaroni R and Brédas J L 1998 *Synth. Met.* **93** 83
[16] Vaschetto M E, Monkman A P and Springborg M 1999 *J. Mol. Struct. (Theochem)* **468** 181
[17] Lim S L, Tan K L, Kang E T and Chin W S 2000 *J. Chem. Phys.* **112** 10648
[18] Foreman J P and Monkman A P 2003 *J. Phys. Chem.* A **107** 7604
[19] Kwon O and McKee M L 2000 *J. Phys. Chem.* B **104** 1686
[20] Cavazzoni C, Colle R, Farchioni R and Grosso G 2002 *Phys. Rev.* B **66** 165110
[21] Cavazzoni C, Colle R, Farchioni R and Grosso G 2005 *Comput. Phys. Commun.* **169** 135
[22] Dávila L Y A and Caldas M J 2001 *Synth. Met.* **119** 241
[23] Can M, Pekmez N Ö and Yildiz A 2003 *Polymer* **44** 2585
[24] Varela-Álvarez A, Sordo J A and Scuseria G E 2005 *J. Am. Chem. Soc.* **127** 11318
[25] Galvão D S, dos Santos D A and Laks B 1989 *Phys. Rev. Lett.* **63** 786
[26] Schulz P A, Galvão D S and Caldas M J 1991 *Phys. Rev.* B **44** 6073
[27] Wu H-L and Phillips P 1991 *Phys. Rev. Lett.* **66** 1366
[28] Farchioni R, Vignolo P and Grosso G 1999 *Phys. Rev.* B **60** 15705
[29] McCall R P, Ginder J M, Leng J M, Ye H J, Manohar S K, Masters J G, Asturias G E, MacDiarmid A G and Epstein A J 1990 *Phys. Rev.* B **41** 5202
[30] Cao Y, Smith P and Heeger A J 1989 *Synth. Met.* **32** 263
[31] Vignolo P, Farchioni R and Grosso G 2001 *Phys. Status Solidi* b **223** 853

[32] Yoder G, Dickerson B K and Chen A-B 1999 *J. Chem. Phys.* **111** 10347
[33] Ginder J M and Epstein A J 1990 *Phys. Rev.* B **41** 10674
[34] Tomfohr J and Sankey O F 2004 *J. Chem. Phys.* **120** 1542
[35] Xu B and Tao N J 2003 *Science* **301** 1221
[36] Ramachandran G K, Tomfohr J K, Li J, Sankey O F, Zarate X, Primak A, Terazono Y, Moore T A, Moore A L, Gust D, Nagahara L A and Lindsay S M 2003 *J. Phys. Chem.* B **107** 6162
[37] He J, Chen F, Liddell P A, Andréasson J, Straight S D, Gust D, Moore T A, Moore A L, Li J, Sankey O F and Lindsay S M 2005 *Nanotechnology* **16** 695
[38] Lewis J P, Glaesemann K R, Voth G A, Fritsch J, Demkov A A, Ortega J and Sankey O 2001 *Phys. Rev.* B **64** 195103
Demkov A A, Ortega J, Sankey O F and Grumbach M P 1995 *Phys. Rev.* B **52** 1618
Sankey O F and Niklewski D J 1989 *Phys. Rev.* B **40** 3979
[39] Baroni S, Corso A D, de Gironcoli S and Giannozzi P http://www.pwscf.org.
[40] Kresse G and Furthmüller J 1996 *Comput. Mater. Sci.* **6** 15
Kresse G and Hafner J 1993 *Phys. Rev.* B **47** 558
Kresse G and Furthmüller J J 1996 *Phys. Rev.* B **54** 11169
[41] Tomfohr J K and Sankey O F 2002 *Phys. Rev.* B **65** 245105
[42] Chang Y-C and Schulman J N 1982 *Phys. Rev.* B **25** 3975
[43] Boykin T B 1996 *Phys. Rev.* B **54** 7670
Boykin T B 1996 *Phys. Rev.* B **54** 8107
[44] Imry Y and Landauer R 1999 *Rev. Mod. Phys.* **71** S306
[45] Li J, Tomfohr J K and Sankey O F 2003 *Physica* E **19** 133
[46] Datta S 1995 *Electronic Transport in Mesoscopic Systems* (Cambridge: Cambridge University Press)
[47] Xue Y, Datta S and Ratner M A 2002 *Chem. Phys.* **281** 151
[48] Landauer R 1989 *J. Phys.: Condens. Matter* **1** 8099
[49] Büttiker M, Imry Y, Landauer R and Pinhas S 1985 *Phys. Rev.* B **31** 6207
[50] Damle P S, Ghosh A W and Datta S 2001 *Phys. Rev.* B **64** 201403
[51] Picaud F, Smogunov A, Corso A D and Tosatti E 2003 *J. Phys.: Condens. Matter* **15** 3731
[52] Schmidt M W, Baldridge K K, Boatz J A, Elbert S T, Gordon M S, Jensen J H, Koseki S, Matsunaga N, Nguyen K A, Su S J, Windus T L, Dupuis M and Montgomery J A 1993 *J. Comput. Chem.* **14** 1347
[53] Leng J M, Ginder J M, McCall R P, Ye H J, Epstein A J, Sun Y, Manohar S K and MacDiarmid A G 1991 *Synth. Met.* **41–43** 1311
[54] Xiao X, Xu B Q and Tao N J 2004 *Nano Lett.* **4** 267